

REPORTS

tion energy partitioned into H_2 excitation (10). In diffuse clouds H_2 formation is thought to occur on the surface of bare carbonaceous and silicate grains. Recent experiments on the formation of interstellar carbon dust grain analogs suggest that these could very well be microporous structures showing nanometer-scale porosity (24). Because H and H_2 are physisorbed on these surfaces (and internal pore surfaces) with similar binding energies to that of ASW, and energy transfer mechanisms between H_2 and the pore surfaces are likely similar (16), we suggest that H_2 retention in pores will be similar on the bare grains to that for ASW. Hence, the energy distribution in H_2 formation could show a similar dependence on dust grain morphology for bare carbonaceous grains as seen here for ASW films. All that is required is that the morphology (pore structure) induces a lifetime on the grain that is long compared with the overall energy relaxation time for the nascent H_2 exoergicity. For silicates, both compact and fluffy grain particles have been found in meteorites and have been grown under laboratory conditions relevant to the ISM. However, the details of the morphology of these grains is unknown, so we can only speculate that the energy budget of H_2 produced on these grains should depend in a similar way to internal morphology as for the ASW films. Therefore, we propose that the dominant effect controlling the initial energy distributions of gas phase H_2 formed in the ISM may not be the detailed chemical nature of the grain surfaces but rather their morphology.

References and Notes

- D. Hollenbach, E. E. Salpeter, *Astrophys. J.* **163**, 155 (1971).
- M. Jura, *Astrophys. J.* **197**, 575 (1975).
- C. Gry *et al.*, *Astron. Astrophys.* **139**, 675 (2002).
- N. Katz, I. Furman, O. Biham, V. Pironello, G. Vidali, *Astrophys. J.* **522**, 305 (1999).
- G. Manico, G. Raguni, V. Pironello, J. Roser, G. Vidali, *Astrophys. J.* **548**, L253 (2001).
- D. R. Flower, G. P. des Forêts, *Mon. Not. R. Astron. Soc.* **247**, 500 (1990).
- W. W. Duley, D. A. Williams, *Mon. Not. R. Astron. Soc.* **260**, 37 (1993).
- J. M. Greenberg, *Surf. Sci.* **500**, 793 (2002).
- E. L. Gibb, D. C. B. Whittet, W. A. Schutte, *Astrophys. J.* **536**, 347 (2000).
- J. Takahashi, K. Masuda, M. Nagaoka, *Astrophys. J.* **520**, 724 (1999).
- H_2O deposition conditions are typically $\sim 45^\circ$ HWHM angular spread and 0.3 to 3 ML/s dose rates.
- K. P. Stevenson, G. A. Kimmel, Z. Dohnalek, R. S. Smith, B. D. Kay, *Science* **283**, 1505 (1999).
- The triply differentially pumped H and D atom beams are formed by microwave discharges with fluxes of $\leq 10^{13}$ atoms $cm^{-2}s^{-1}$, beam dissociation probabilities of $\sim 65\%$, and Maxwell-Boltzmann kinetic energy distributions of $T = 300$ K. The H and D beams are incident upon the ASW surface at 0° and 4° relative to the surface normal and are overlapped at the center of the ASW surface with beam diameters of 1.5 mm and 3.5 mm, respectively.
- TPD measurements are performed by heating the sample with a linear ramp (typically 0.5 K/s) using electron bombardment on the back side of the Cu substrate and simultaneously detecting the desorption of HD, H_2 , and D_2 from the front of the ASW surface with a differentially pumped quadrupole mass spectrometer (QMS) with an aperture close to the ASW surface to limit the field of view in the TPD. LITD measurements were performed by inducing a temperature jump of typically 20 ns on the surface using a 200 μJ laser pulse at 532 nm focused to a 1.5 mm diameter spot at the center of the overlapped atom beams. The kinetic energy distribution of molecules desorbing during the temperature jump are obtained from the TOF distributions to another differentially pumped mass spectrometer placed 10 cm from the surface (27).
- L. Hornekær, A. Baurichter, V. Petrunin, B. Kay, A. Luntz, in preparation.
- The desorption yield and TPD spectra for HD were unaffected by repeated cycling of H+D adsorption experiments on the same ASW film, indicating that little restructuring of the ASW pore structure takes place as a result of the release of the recombination energy. Hence, the retention of HD molecules in ASW pores is not caused by pore collapse and volcano formation, as seen for more tightly bound adsorbates exhibiting rapid low-temperature thermal diffusion (25), but is simply due to the fact that particles desorbing from pore surfaces in the porous network have to undergo a series of adsorption-desorption cycles before making their way to the external film surface, from which desorption into the gas phase can take place.
- The distinction between the Langmuir-Hinshelwood (LH) and hot atom reaction mechanisms is in the origin of atom mobility on the 10 K surface. In the LH mechanism, this is caused by thermal atom diffusion, whereas in the hot atom mechanism this is caused by transient mobility on the surface during the adsorption process, i.e., before the atom fully thermalizes on the surface. All experiments reported here are consistent with both mechanisms. Our bias is that the LH mechanism dominates because of the absence of H coverage dependence in apparent rates of recombination and because it is hard to rationalize HD retention in the internal porous surface if hot atom reaction occurs on the external surface.
- The small residual signal in Fig. 2 is thought to arise from recombination of atoms trapped at the Cu-substrate-ASW interface.
- $S_{D_2} = 0.6 \pm 0.10$ for porous ASW and $S_{D_2} = 0.20 \pm 0.15$ for nonporous ASW at $T_s \sim 8$ K, as obtained by the King and Wells method.
- S. Andersson, L. Wilzen, M. Persson, J. Harris, *Phys. Rev. B* **40**, 8146 (1989).
- L. Diekhöner, H. Mortensen, A. Baurichter, A. C. Luntz, *J. Chem. Phys.* **115**, 3356 (2001).
- H. C. Chang, G. E. Ewing, *J. Electron Spectrosc.* **54**, 39 (1990).
- M. Bonn, M. J. P. Brugmans, A. W. Kleyn, R. A. van Santen, *Chem. Phys. Lett.* **233**, 309 (1995).
- M. Schnaier *et al.*, *Astrophys. J.* **519**, 687 (1999).
- M. P. Collings, J. W. Deaver, H. J. Fraser, M. R. S. McCoustra, D. A. Williams, *Astrophys. J.* **583**, 1058 (2003).
- Supported by The Danish National Research Council (grant no. 21000269), the Danish National Research Foundation through the Aarhus Center of Atomic Physics, and the Carlsberg Foundation. We thank B. Kay and A. Andersen for useful discussions and advice.

26 August 2003; accepted 11 November 2003

Fault Interactions and Large Complex Earthquakes in the Los Angeles Area

Greg Anderson,*† Brad Aagaard,‡ Ken Hudnut

Faults in complex tectonic environments interact in various ways, including triggered rupture of one fault by another, that may increase seismic hazard in the surrounding region. We model static and dynamic fault interactions between the strike-slip and thrust fault systems in southern California. We find that rupture of the Sierra Madre-Cucamonga thrust fault system is unlikely to trigger rupture of the San Andreas or San Jacinto strike-slip faults. However, a large northern San Jacinto fault earthquake could trigger a cascading rupture of the Sierra Madre-Cucamonga system, potentially causing a moment magnitude 7.5 to 7.8 earthquake on the edge of the Los Angeles metropolitan region.

Faults interact with each other over a variety of temporal and spatial scales. Long-term interactions through static stress transfer have been observed in Turkey, Alaska, California, Japan, and elsewhere, whereas dynamic rupture propagation from one fault to another during a single event has been seen in several recent large earthquakes (1–3). Although these studies have largely concentrated on strike-slip faults, some large events—including the 1957 moment magnitude (M_w) = 8.3 Gobi-Altay (4) and 2002

M_w = 7.9 Denali Fault, Alaska (5, 6), earthquake sequences—involved interactions between thrust and strike-slip fault systems. Many heavily populated regions contain thrust and strike-slip fault networks, so understanding the mechanisms by which faults in such networks interact is critical for improved estimates of seismic hazard and risk in those areas.

The northern edge of the densely populated Los Angeles metropolitan region is bounded by the Sierra Madre-Cucamonga (SMF-CF) thrust fault system, which produced the M_w = 6.7 1971 San Fernando earthquake and may generate events up to M_w = 7.5 (7). To the east and north lie the San Andreas (SAF) and San Jacinto (SJF) right-lateral strike-slip fault systems; each may slip in events exceeding M_w = 7.0, and events of M_w = 7.8 occurred on the SAF in 1685 and 1857 (8). Here, we examine

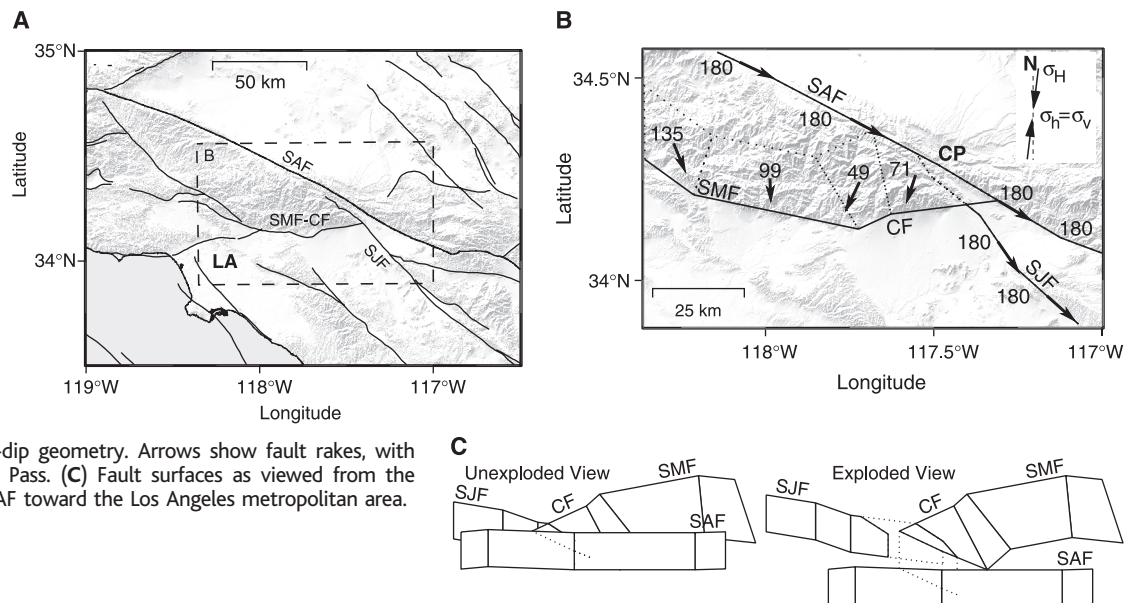
U.S. Geological Survey, 525 South Wilson Avenue, Pasadena, CA 91106–3212, USA.

†Present address: UNAVCO, 6350 Nautilus Drive, Boulder CO 80301, USA.

‡Present address: U.S. Geological Survey, 345 Middlefield Road, M/S 977, Menlo Park CA 94025, USA.

*To whom correspondence should be addressed. E-mail: anderson@unavco.org

Fig. 1. Study region and fault geometry. (A) Southern California study region, with shaded relief in background. Thin lines: regional faults; dashed box: region in (B). LA: Los Angeles; SAF: San Andreas fault; SJF: San Jacinto fault; SMF: Sierra Madre fault; CF: Cucamonga fault. (B) Fault geometry, regional stress orientation, and fault rakes due to regional stress, with shaded relief in background. Heavy solid lines show surface fault traces, dotted lines show surface projections of down-dip geometry. Arrows show fault rakes, with values in degrees. CP: Cajon Pass. (C) Fault surfaces as viewed from the northeast looking over the SAF toward the Los Angeles metropolitan area.



past and potential ruptures on the SAF, SJF, CF, and SMF (Fig. 1 and Table 1) (9). We model both static stress transfer between separate events and dynamic rupture propagation during a single event, so that we can understand a wider range of possible fault interactions. In doing so, we find faults whose ruptures encourage ruptures of other faults at later times, as well as sets of faults that may fail in a single, large, complex event.

To model static stress interactions, we create kinematic rupture models (10) for scenario earthquakes (see supporting text). We then use these models and the theory of deformation from dislocations in a homogeneous elastic half-space to compute coseismic stress increment tensors at regularly spaced points on target fault planes. We resolve these tensors into shear, normal, and Coulomb stress changes. The change in Coulomb stress is $\Delta CFS = \Delta\tau + \mu' \Delta\sigma$, where $\Delta\tau$ is the coseismic change in shear stress in the direction of fault slip, $\Delta\sigma$ is the change in normal stress (with tension positive), and μ' is the effective coefficient of friction, accounting for pore-fluid pressure effects. This general technique has been widely used to model static stress interactions in earthquake sequences (1–3), and typically, $\Delta CFS \geq 0.01$ to 0.02 MPa has been associated with observable changes in seismicity rate, although smaller stress changes may also play a role.

Our dynamic rupture models (10) solve the dynamic elasticity equations, incorporating fracture physics and frictional sliding, to produce time histories of fault slip and seismic waves. We follow the same general methodology of our previous work with dynamic rupture models (11–13). We use a three-dimensional tetrahedral finite-element model that includes material property variations with depth (table S3) and captures seis-

Table 1. Summary of the potential for static and dynamic interactions among major faults considered in this study. Upper panel summarizes potential long-term interactions through static stress transfer; lower panel summarizes possible propagating ruptures. Yes: rupture propagation or positive Coulomb stress transfer between faults; No: no rupture propagation or negative Coulomb stress transfer between faults; Maybe: rupture propagation or Coulomb stress transfer depends on geometry of SJF/SAF and SJF/CF intersections (9); Unclamped: strong tensile normal stress, which may be important for thrust faults (16).

Rupture of...	Encourages rupture of...			
	San Andreas	San Jacinto	Cucamonga	Sierra Madre
	<i>Static modeling</i>			
SAF NW	–	Yes	Unclamped	Unclamped
SAF SE	–	No	Yes	Unclamped
San Jacinto	NW: Yes, SE: No	–	Maybe	No effect
Cucamonga	Unclamped	Yes	–	Yes
Sierra Madre	Unclamped	No effect	Yes	–
	<i>Dynamic modeling</i>			
SAF NW	–	Maybe	No	No
SAF SE	–	No	No	No
San Jacinto	Maybe	–	Maybe	Maybe
Cucamonga	No	No	–	Yes
Sierra Madre	No	No	Yes	–

mic waves with periods of 2.0 s and longer. We assume that the faults are critically loaded so that ruptures propagate to the fullest extent possible, as determined by the fault geometry and shear stress orientation. We nucleate ruptures on the various faults and examine whether the ruptures propagate onto neighboring faults, indicating the potential for complex events.

We start by modeling the effect on the San Andreas and San Jacinto faults of a Cucamonga fault event. Figure 2A shows that our static model with an $M_w = 7.0$ scenario CF event generates $\Delta CFS \geq 0.1$ MPa on the SMF, the San Bernardino Valley segment of the SJF, and the SAF near Cajon Pass; however, ΔCFS is negative both northwest and southeast of Cajon Pass. Normal stress changes (not shown) are strongly negative

(less than -0.1 MPa) along the SMF and strongly positive (more than 0.5 MPa) along the SAF near Cajon Pass. Thus, rupture of the CF encourages rupture of the northern SJF and the SMF and strongly unclamps the SAF near Cajon Pass.

The dynamic model agrees with this scenario: A rupture nucleating on the western CF easily expands onto the SMF and the eastern CF (Fig. 2B and movie S1), whereas on the other faults, seismic waves generate large shear stress changes that do not reach the failure threshold of 5 to 9 MPa above the initial stress. The rate-dependent friction creates an abrupt increase in friction as the slip rate drops, which generates small length-scale heterogeneities in the postslip stress field. As the rupture nears the SJF, it increases shear stress on the SJF above or north of

REPORTS

the CF (hanging wall side), but decreases shear stress below or south (footwall side) of the CF by up to 5 MPa. Stress changes on the SAF are similar. Thus, the left-lateral oblique motion on the CF inhibits dynamic triggering of rupture on the SAF and SJF, but promotes dynamic rupture propagation onto the SMF.

We also consider whether a San Andreas fault rupture might trigger Cucamonga or San Jacinto fault rupture (Table 1). We first model

an $M_w = 7.0$ event on the SAF, rupturing the segment from Banning Pass to Cajon Pass. Static modeling indicates that such an event is more likely to encourage rupture of the CF than of the SJF, because $\Delta CFS < 0.1$ MPa along most of the SJF north of Anza, discouraging rupture of the SJF, while $\Delta CFS \geq 0.05$ MPa over much of the eastern CF.

In the dynamic model, rupture begins near Banning Pass and propagates northwest. We

reduce the shear stress on the northwestern SAF to force rupture termination just north of Cajon Pass, similar to the 1685 event. As rupture propagates northward, it reduces shear stress by 1 MPa over much of the SJF, although the seismic waves momentarily generate small shear stress increases (movie S2). As the seismic waves reach the eastern portion of the CF, the shear stress fluctuations are strong but insufficient to trigger slip. Consequently, a rupture on the SAF with a northern termination similar to the 1685 rupture would probably not trigger simultaneous CF rupture; doing so requires an abrupt decrease in SAF slip close to a portion of the CF that is already close to nucleating its own rupture.

Another possible triggering scenario is a repeat of the $M_w = 7.8$ 1857 Fort Tejon earthquake on the San Andreas fault. Using an updated 1857 slip distribution (14), we compute stress changes on the other faults. ΔCFS exceeds 0.05 MPa on the northern SJF, encouraging rupture; this is consistent with earlier work (15) hypothesizing triggered slip on the SJF during the 1857 event. ΔCFS is negative along the Cucamonga and Sierra Madre faults, but normal stress changes exceed 0.5 MPa along the CF and eastern SMF; if normal stress changes are important for thrust faults (16), then a repeat of the 1857 event would encourage rupture of those faults (Table 1).

We nucleate dynamic rupture near the center of the northwestern portion of the SAF and force it to end near Cajon Pass by reducing shear stress on the SAF southeast of that point. As rupture propagates southeastward, shear stress on the western CF drops by up to 4 MPa. When rupture approaches the intersection with the SJF, shear stress changes on the SJF fall just below the failure threshold, and rupture does not propagate onto the SJF; however, only small perturbations in the geometry or stress field would lead to rupture propagation. These results suggest that the SJF may rupture simultaneously during a repeat of the 1857 SAF event, but that the SMF-CF system is less likely to do so.

We also examine the effect of San Jacinto fault rupture on the Cucamonga and San Andreas faults by modeling an $M_w = 7.1$ event rupturing the northern 60 km of the SJF (Fig. 3 and Table 1). Because of large static shear stress increases, ΔCFS exceeds 0.1 MPa along the SAF from Wrightwood to about Palmett Creek, suggesting a strong tendency for coupled rupture of the northern SJF and the Mojave segment of the SAF; strongly negative ΔCFS southeast of Cajon Pass tends to inhibit rupture there. Our dynamic model, with rupture nucleating near the southern end of our SJF segment, gives similar results. As the rupture progresses northward, it casts a stress shadow on the SAF southeast of Cajon Pass (Fig. 3B and movie S4), whereas shear stress increases northwest of Cajon Pass. If

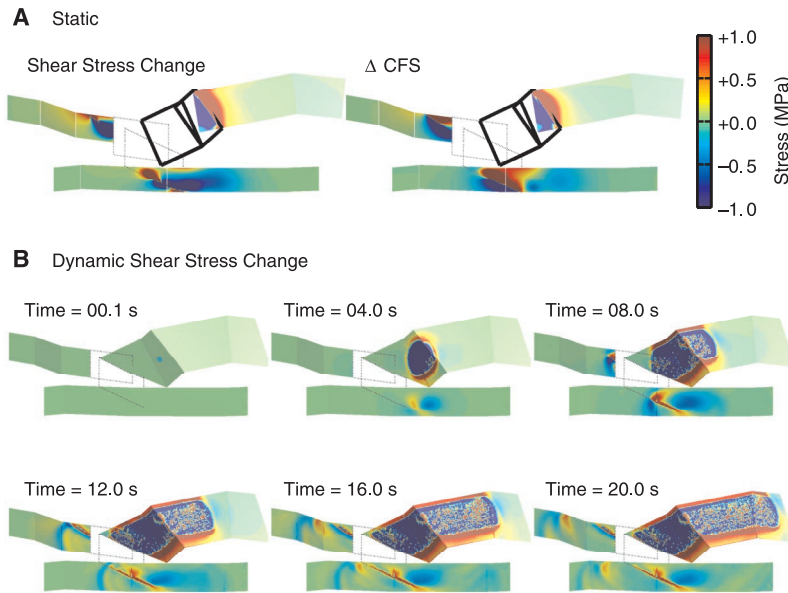


Fig. 2. (A) Static shear and Coulomb stress changes from an $M_w = 7.0$ earthquake on the Cucamonga fault. CF rupture encourages rupture of the Sierra Madre and northern San Jacinto faults, and strongly unclamps the San Andreas fault near Cajon Pass. Open rectangles show location of the CF. (B) Snapshots of shear stress change from an $M_w = 7.4$ earthquake on the CF and SMF. Strong negative dynamic stress changes prevent propagation onto the SJF or SAF.

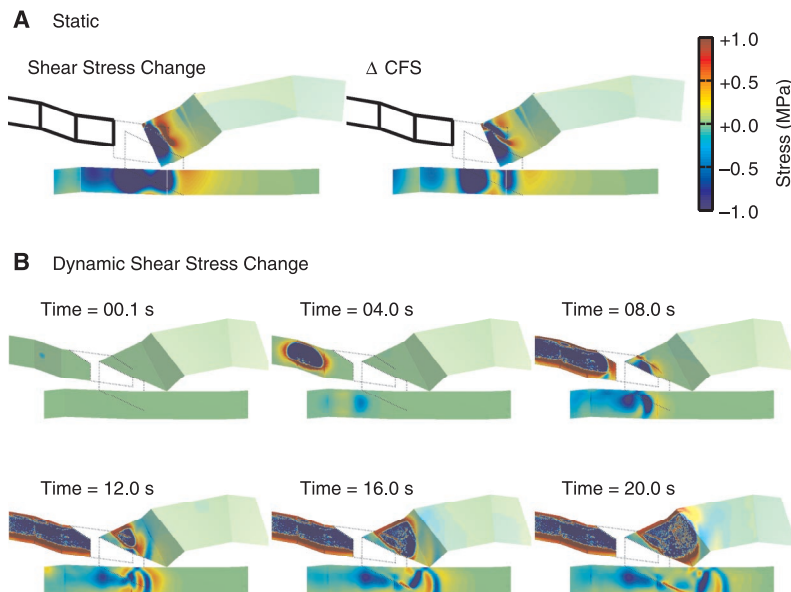


Fig. 3. (A) Static shear and Coulomb stress changes from an $M_w = 7.1$ earthquake on the San Jacinto fault. Rupture of the northern SJF may encourage rupture of the Cucamonga fault, depending on the geometry, and encourages rupture of the Mojave segment of the San Andreas fault. (B) Snapshots of shear stress change from an $M_w = 7.5$ earthquake on the San Jacinto, Cucamonga, and Sierra Madre faults. SJF rupture propagates onto CF and SMF.

the SJF rupture proceeds to within a few kilometers of the SAF, the rupture continues northward on the SAF. Thus, a large northern SJF event may trigger SAF rupture, perhaps similar to the $M_w = 7.5$ 1812 event (17) or even the $M_w = 7.8$ 1857 earthquake.

Our static modeling of a San Jacinto fault event shows that such an event also causes large positive ΔCFS along the Cucamonga fault, encouraging coupled rupture of the CF and northern SJF. If the SJF ends at the CF, and ≥ 3 m of slip is generated at the northern end of the fault, our dynamic models indicate that rupture will jump onto the CF and propagate toward the west (Fig. 3B and movie S4). Because both static and dynamic stress changes from a CF rupture are positive along the central and eastern Sierra Madre fault, an SJF event could become a cascading rupture of the full SMF-CF system. This earthquake would have a combined rupture length of about 200 km and $M_w = 7.5$ to 7.8. The faults involved are closer to the densely populated Los Angeles metropolitan region than is the SAF, so although the predominantly along-strike rupture of the SMF-CF system would tend to moderate the near-source velocity pulses associated with rupture directivity (18),

ground motion and damage would possibly exceed those generated by a repeat of the 1857 earthquake. This is among the worst-case scenario earthquakes for southern California.

References and Notes

1. R. A. Harris, *J. Geophys. Res.* **103**, 24347 (1998).
2. R. S. Stein, *Nature* **402**, 605 (1999).
3. G. C. P. King, M. Cocco, *Advances in Geophysics*, R. Dmowska, Ed. (Academic Press, New York, 2000), vol. 44, pp. 1–36.
4. R. A. Kurushin *et al.*, "The surface rupture of the 1957 Gobi-Altay, Mongolia, earthquake," *Geol. Soc. Am. Spec. Pap.* **320** (Geological Society of America, Boulder, CO, 1997).
5. D. Eberhart-Phillips *et al.*, *Science* **300**, 1113 (2003).
6. G. Anderson, C. Ji, *Geophys. Res. Lett.* **30**, 10.1029/2002GL016724 (2003).
7. C. M. Rubin, S. C. Lindvall, T. K. Rockwell, *Science* **281**, 398 (1998).
8. T. E. Fumal *et al.*, *Bull. Seismol. Soc. Am.* **92**, 2726 (2002).
9. We approximate the CF, SAF, SJF, and SMF by 15 planar surfaces based on the Southern California Earthquake Center (SCEC) Community Fault Model (19). Due to great uncertainty in the termination of the SJF and CF, we consider two variations of the geometry: The SJF ends at the CF, and the SJF penetrates through the CF.
10. In the static kinematic rupture models, we prescribe the magnitude and orientation of the slip on our faults. In the dynamic rupture models, the magnitude and orientation of fault slip develop as a result of solving the elastodynamic equations with the specified friction boundary conditions on the fault surfaces.
11. Supporting online material is available on *Science Online*.
12. B. T. Aagaard, "Finite-element simulations of earthquakes," *Tech. Rep. 99-03* (California Institute of Technology, Earthquake Engineering Research Laboratory, Pasadena, CA, 1999).
13. B. T. Aagaard, T. H. Heaton, J. F. Hall, *Bull. Seismol. Soc. Am.* **91**, 1765 (2001).
14. J. Lin, R. S. Stein, *J. Geophys. Res.* in press.
15. F. F. Pollitz, I. S. Sacks, *Bull. Seismol. Soc. Am.* **82**, 454 (1992).
16. T. Parsons, R. S. Stein, R. W. Simpson, P. A. Reasenberg, *J. Geophys. Res.* **104**, 20183 (1999).
17. T. R. Topozada, D. M. Branum, M. S. Reichle, C. L. Hallstrom, *Bull. Seismol. Soc. Am.* **92**, 2555 (2002).
18. B. T. Aagaard, J. F. Hall, T. H. Heaton, *Bull. Seismol. Soc. Am.*, in press.
19. A. Plesch, J. H. Shaw, *Eos Trans. AGU* **83**, abstract S21A-0966 (2002).
20. The Center for Advanced Computing Research provided access to the Hewlett-Packard V-Class computer at the California Institute of Technology. We thank R. Stein for sharing his updated slip model for the 1857 earthquake and R. Harris, K. Kendrick, N. King, and two anonymous reviewers for critical reviews, which improved this manuscript.

Supporting Online Material

www.sciencemag.org/cgi/content/full/302/5652/1946/DC1

SOM Text

Figs. S1 and S2

Tables S1 to S3

Movies S1 to S4

References

25 August 2003; accepted 11 November 2003

Doubly Ionized Carbon Observed in the Plasma Tail of Comet Kudo-Fujikawa

Matthew S. Povich,^{1*} John C. Raymond,¹ Geraint H. Jones,² Michael Uzzo,¹ Yuan-Kuen Ko,¹ Paul D. Feldman,³ Peter L. Smith,¹ Brian G. Marsden,¹ Thomas N. Woods⁴

Comet C/2002 X5 (Kudo-Fujikawa) was observed near its perihelion of 0.19 astronomical unit by the Ultraviolet Coronagraph Spectrometer aboard the Solar and Heliospheric Observatory spacecraft. Images of the comet reconstructed from high-resolution spectra reveal a quasi-spherical cloud of neutral hydrogen and a variable tail of C^+ and C^{2+} that disconnects from the comet and subsequently regenerates. The high abundance of C^{2+} and C^+ , at least 24% relative to water, cannot be explained by photodissociation of carbon monoxide and is instead attributed to the evaporation and subsequent photoionization of atomic carbon from organic refractory compounds present in the cometary dust grains. This result serves to strengthen the connection between comets and the material from which the Solar System formed.

The first evidence for the existence of the solar wind came from observations of the tails of comets, and comets continue to

serve as natural probes of the heliospheric environment (1). Comets are among the most primitive objects in the Solar System. Cometary nuclei are small (most are a few kilometers in diameter), solid bodies composed of dust and ices accumulated directly from the protoplanetary disk and preserved in the cold outer reaches of the Solar System. As a comet approaches the Sun, sublimation of the ices forms an extended gas cloud (the coma) around the nucleus along with distinctive dust and plasma tails that can extend for 10^8 km. Spectroscopy has

revealed the composition of these objects and their interaction with the interplanetary environment, but many mysteries remain.

Comet C/2002 X5 (Kudo-Fujikawa) was discovered on 14 December 2002 by two Japanese amateur astronomers (2, 3). Its calculated orbit placed its perihelion at 0.19 astronomical unit (AU) (1 AU = 1.496×10^{11} m, the average Earth-Sun distance) on 29 January 2003 at 00:15 universal time (UT). This close approach to the Sun provided a favorable geometry for observing Kudo-Fujikawa with the Ultraviolet Coronagraph Spectrometer (UVCS) (4), an instrument on board the SOHO (Solar and Heliospheric Observatory) spacecraft. UVCS is a long-slit spectrograph operating in the ultraviolet wavelength range of 94 to 130 nm (in first order). The length of the UVCS slit gives a field of view of 41 arc min. At perihelion, comet Kudo-Fujikawa was on the far side of the Sun from SOHO, so its elongation was small enough to allow UVCS to observe it from 19:00 UT on 27 January 2003 until 07:00 UT on 29 January 2003. The UVCS slit was placed at 11 different positions in the path of the comet, and spectra were obtained in 120-s exposures as the comet crossed the slit. The first and last crossings were the most favorable for spectroscopic imaging of Kudo-Fujikawa, because at these times the orientation of the slit gave the largest angles between the slit and the velocity of the comet. For these data sets, the spectral bandpasses were 97.3 to 98.8 nm and 120.9 to 122.3 nm,

¹Harvard-Smithsonian Center for Astrophysics, 60 Garden Street, Cambridge, MA 02138, USA. ²Jet Propulsion Laboratory, 4800 Oak Grove Drive, Pasadena, CA 91109, USA. ³Department of Physics and Astronomy, Johns Hopkins University, 3400 North Charles Street, Baltimore, MD 21218–2686, USA. ⁴University of Colorado, Laboratory for Atmospheric and Space Physics, 1234 Innovation Drive, Boulder, CO 80303, USA.

*To whom correspondence should be addressed. E-mail: mpovich@cfa.harvard.edu